J Nanopart Res (2017) 19: 200
DOI 10.1007/s11051-017-3871-1

RESEARCH PAPER

Enhanced photocatalytic activities of low-bandgap TiO_2-reduced graphene oxide nanocomposites

Ying Chen · Xinju Dong · Yan Cao · Junjie Xiang · Hongyan Gao

Received: 23 July 2016 / Accepted: 26 April 2017 / Published online: 3 June 2017

Abstract In this study, a hydrothermal method was successfully used to prepare a reduced graphene oxide (RG)–titanium dioxide (TiO_2) hybrid in 10–20 nm, starting from commercial TiO_2 P25 nanoparticles and liquid-exfoliated graphene oxide (GO). Compared to TiO_2, an obvious red shift of light absorption (from 3.1 to 2.6 eV) of the as-prepared RG–TiO_2 was observed by UV–Vis analysis, and an enhanced photocatalytic degradation of the Rhodamine B (Rh. B) was also observed under Xe lamp exposure test by using the as-prepared RG–TiO_2. Multiple characterizations of this RG–TiO_2 nanocomposite confirmed that its photocatalytic enhancement could be ascribed to two approaches. Firstly, RG extended the mean free path and photogenerated electrons' lifetime of TiO_2, which minimized electron–hole pairs' recombination. Secondly, RG expanded the light absorption spectrum of TiO_2 from UV range to UV and visible light range. The explication of these improvements was concluded as the energy gap changing and a likelihood of up-conversion photoluminescence mechanism (UCPL). Due to the low-cost, nonpoisonous and excellent photocatalytic properties of RG–TiO_2, this material can be applied well in sewage treatment and other related fields.

Y. Chen · X. Dong · Y. Cao (✉) · J. Xiang · H. Gao
Institute for Combustion Science and Environmental Technology, Department of Chemistry, Western Kentucky University, Bowling Green, KY 42101, USA
e-mail: yan.cao@wku.edu

Keywords TiO_2 · Graphene · Photocatalyst · Low-bandgap · Up-conversion photoluminescence · Nanocomposites · Sewage treatment

Introduction

With outstanding physicochemical properties, semiconductor nanocrystals are thought to be ideally potential materials applied in electronic devices, energy conversion devices, supercapacitors, photocatalysts, etc. Among them, titanium dioxide (TiO_2), as a nontoxic, low-cost, long-term stable, and highly efficient photocatalyst, is well developed in photovoltaics (Kim et al. 2003), dye-sensitized solar cell (DSSC) (Tributsch 1972), water splitting (Fujishima and Honda 1972), solar fuel producing (Yamashita et al. 1994), ionic pollutants treatment (Yue 2015 #169), and other photocatalytic reactions. Moreover, TiO_2 can also be used as an environmental cleanup material for antimicrobial and self-cleaning applications using solar energy (Anandan et al. 2012; Chien et al. 2011; Jiang et al. 2011; Mir et al. 2013; Pelizzetti et al. 1992; Wu et al. 1998). However, as a photocatalyst, TiO_2 also meets some limitations. First of all, the bandgap of TiO_2 (3.2 eV) can only respond to ultraviolet (UV) light (about 3–5% of sunlight). Meanwhile, the relatively high intrinsic electron–hole recombination of TiO_2 further decreases its utilization efficiency of light. Besides, as in the self-cleaning applications, the recovery of TiO_2 nanoparticles from treated water is also difficult. To overcome these disadvantages, TiO_2 has been co-synthesized with numerous

types of materials, such as Ag (Cozzoli et al. 2004), Au (Subramanian et al. 2003), and ZnO (Liao et al. 2008) to achieve an inside doping or a surface decoration. Recently, with swift developments of carbon nanomaterials, more and more interest has been paid to promising carbon–TiO_2 composites.

Graphene and its analogues, such as graphene oxide (GO) and reduced graphene oxide (RG), have become very popular recently, with great charge carrier mobility (105 cm^2 Vs^{-1} at an ambient temperature and 106 cm^2 Vs^{-1} at low temperatures; Sun and Chang 2014) and thermal conductivity (up to ~5000 W mK^{-1} for the suspended single-layer graphene at room temperature; Sun and Chang 2014). Hence, many works have focused on the synergetic effect of TiO_2 with graphene materials in photocatalytic applications (Fan et al. 2011; Huang et al. 2013; Jiang et al. 2014; Long et al. 2013; Ong et al. 2014; Pan et al. 2015, 2012; Perera et al. 2012; Qian et al. 2014; Ramadoss and Kim 2013; Sher Shah et al. 2012; Wang et al. 2013; Zhang et al. 2009, 2011a, 2010; Zhu et al. 2015). There was also a good recently updated review that pointed out two key factors of high-performance photocatalytic systems, which were efficient light absorption and charge separation of applied photocatalysts (Wang et al. 2017). However, studies are rare on the interfacial interaction between TiO_2 and graphene materials, which may play important roles in better understanding enhanced visible light utilization. Thus, this study focused on analyzing the Ti–O–C chemical bond between TiO_2 and RG interfaces in a hydrothermally synthesized RG–TiO_2 nanocomposite, and its improved photocatalytic activity in the photodegrading Rh. B. Sufficient characterization methods have been applied for assisting in elaborate discussion towards a mechanism-level understanding.

Experimental section

Chemicals

All chemicals used were of analytical grade and used without any further purification. Among them, sodium nitrate ($NaNO_3$, extra pure) and Rh. B were purchased from Acros Organics Corporation. Sulfuric acid (H_2SO_4), hydrogen peroxide (H_2O_2; 30%), graphite powder, potassium permanganate ($KMnO_4$), and sodium hydroxide (NaOH) were all purchased from Fisher Scientific Corporation. Aeroxide titania P25 (TiO_2; ca. 80% anatase and 20% rutile) was purchased from Evonik Degussa Corporation. To give a comparative trail, the commercial few layered graphene powder (GP) was purchased from Hefei Vigon Material Technology Co., Ltd. Throughout this entire study, deionized (DI) water was always used.

Synthesis of GO

GO was synthesized from graphite using modified Hummers method (Marcano et al. 2010). First, 1 g of GP and 1 g of $NaNO_3$ were put into 45 mL of concentrated H_2SO_4. Then, 6 g of $KMnO_4$ was gradually added into the solution with vigorous stirring and ice bath to keep the temperature of the mixture below 30 °C 10 min later, the ice bath was changed into water bath, and the mixture was stirred at 35 °C for 4 h. After the color of the ropy mixture turned to dark brown, 200 mL of DI water was slowly poured into the mixture. After continuously stirring for 1 h, the water bath was changed into oil bath and the mixture was then stirred at 98 °C for two more hours. Then, 30 mL of 30% H_2O_2 was carefully added to the mixture. When the color of the mixture fully turned to brown, the mixture was transferred into a large beaker, and then washed with DI water to remove other ions.

Synthesis of RG–TiO_2

Supported by other research study, we chose RG/TiO_2 as 5% of previous research's best practices (Xiang et al. 2012). Ten milliliters of concentrated GO solution (~150 mg GO) was firstly dissolved in 500 mL DI water, and then put under ultrasonic dispersion for about 5 h. To anchor TiO_2 particles onto the surfaces of GO, 100 mL of the diluted solution was taken out and vigorously stirred in a Teflon container, and then 0.5 g of TiO_2 powder was gradually added into the solution. The color change from brown to gray yellow can be clearly seen. Since it is found that sodium hydroxide can help change GO into graphene due to the oxidative debris on GO's surface, 3 g of sodium hydroxide was then added into the solution. After 10 h of vigorous stirring, the Teflon container was transferred to a stainless steel reaction kettle, and kept under 120 °C for 24 h. The color of the GO and TiO_2 mixed dispersion turned to dark gray after the hydrothermal treatment, which may be owing to the transformation of GO into RG. An additional experiment of TiO_2 hydrothermal treatment

without GO has also been done. The color of TiO_2 P25 nanoparticles stayed white, which proved that the color changing from brown to gray should not be caused by titanate formation, or by titania reduction (Zhu et al. 2005). The RG–TiO_2 composite was then washed with DI water and dried under 60 °C.

Synthesis of RG

To make a contrast analysis, individual RG nanosheets were also synthesized separately using the same method as RG–TiO_2. One hundred milliliters of the diluted GO solution was poured into a Teflon container under vigorous stirring, and 3 g of NaOH was gradually added into the solution. Then, after 10 h of vigorous stirring, the as-prepared precursor was also treated under 120 °C for 24 h. Finally, the RG product was washed and dried similar to what was done to RG–TiO_2 composite.

Characterization

For each of samples, X-ray diffraction (XRD; ARL™ X 'TRA Powder Diffractometer, Cu Kα radiation, $\lambda = 1.5406$ Å) was recorded at room temperature with a scan step of 0.02 and a scanning speed of 0.2 s $step^{-1}$. Scanning electron microscopy (SEM; Model JSM-6510LV, JEOL Ltd., Tokyo, Japan) and high-resolution transmission electron microscopy (HRTEM; Model JEM-1400Plus, JOEL Ltd., Tokyo, Japan) were used to characterize the morphologies and size of the synthesized samples. The chemical composition was investigated by the energy dispersive X-ray spectroscopy (EDX). Raman spectra of samples were collected using a DXR Raman microscope (Thermo DXR), including a 780-nm excitation laser and a confocal microscope. The Fourier transform infrared spectra were recorded by FT-IR Spectrometer (PerkinElmer, Spectrum Two) from 4000 to 500 cm^{-1}. The X-ray photoelectron spectroscopy (XPS) measurements were performed with a multi-functional photoelectron spectrometer (Axis Ultra DLD, Kratos) using Al Kα radiation. UV–Vis diffuse-reflectance spectroscopy (DRS) spectra were recorded with a UV–Vis spectrophotometer (Cary, 100 Bio) at wavelengths in the range of 200–800 nm, with a baseline corrected by barium sulfate ($BaSO_4$) powder. Photoluminescence (PL) spectra were measured by fluorescence spectrometer (PerkinElmer, LS 55) using the holder for solids. The heat flow and weight loss curves were measured in air atmosphere by simultaneous differential scanning calorimetry and thermogravimetric analysis (SDT; TA Instrument, 2960 Simultaneous DSC-TGA). BET surface area analysis was carried out using the N2 adsorption isotherms at 77 K by a Micromeritics ASAP 2020 apparatus in the relative pressure range between 0.05 and 0.2.

Electrochemical measurement

For the electrochemical impedance spectroscopy (EIS) measurement, the as-prepared RG–TiO_2 nanocomposite and TiO_2 P25 nanoparticles were fixed to foamed nickel electrodes by the following method: First, to prepare an active material mud, the hybrids, carbon black (Super-P), and polytetrafluoroethylene (PTFE) were ground in an agate mortar at a weight ratio of 8:1:1. The resulting muds were coated onto the nickel foams as the current collectors. Subsequently, the electrodes were dried under ambient condition at 60 °C for 24 h to evaporate the solvent. The EIS measurements were carried out in 0.5 M Na_2SO_4 solution by using a three-electrode system on Zennium electrochemical workstation (Zahner, INC. Germany). The as-prepared resultant electrode served as the working electrode, with a platinum foil as the counter electrode, and a saturated calomel electrode as the reference electrode. The impedance spectra were recorded under an AC perturbation signal of 5 mV over the frequency range of 0.01 to 100,000 Hz at the initial potential of working electrode material.

Rhodamine B Photodegradation

The photodegradation tests of Rh. B using different samples were conducted in a quartz vessel under visible light irradiation which was produced by an arc lamp housing (Newport, Xe lamp, 300 W). In three comparative trails, none of photocatalyst, 10 mg of TiO_2 P25 nanoparticles, and 10 mg of RG–TiO_2 nanocomposite were suspended in 50 mL of Rh. B. solution (30 mg L^{-1}). Before irradiation, the suspensions were stirred in dark for half an hour to obtain an adsorption–desorption equilibrium. Then, the quartz vessel was exposed to the visible irradiation under ambient condition. At every 10 min during the experiment, about 3 mL of mixed solution was collected and analyzed by UV–Vis spectrophotometer (Cary, 100 Bio) for its residual contaminant concentration. The concentration of Rh. B solution was determined by its main peak of the adsorption spectrum at 554 nm. The percentage of degradation is

reported as C/C_0, where C is the absorption of dye solution at each irradiated time interval, while C_0 is the absorption of the initial concentration.

Results and discussion

Material characterization

In the SEM images (Fig. 1a, b), the diameter of nanoparticles was found to be about 10 to 20 nm, which was close to the original size of TiO_2 P25, with a sheet-like material covering those TiO_2 nanoparticles. The corresponding EDX spectrum (Fig. 2a) shows the availability of Ti, O, and C, corresponding to TiO_2 nanoparticles, and the sheet-like RG, respectively. The TEM images (Fig. 1c, d) further revealed the heterostructure of this RG–TiO_2 nanocomposite, showing that TiO_2 nanoparticles (the dark area) are wrapped by a sheet-like structure with wrinkles which is supposed to be RG. The lattice fringes of both TiO_2 and graphene are further evidenced in the HRTEM images (Fig. 1e). The area circled using red short dash in the Fig. 1e with an average lattice size of 0.35 nm were attributed to the

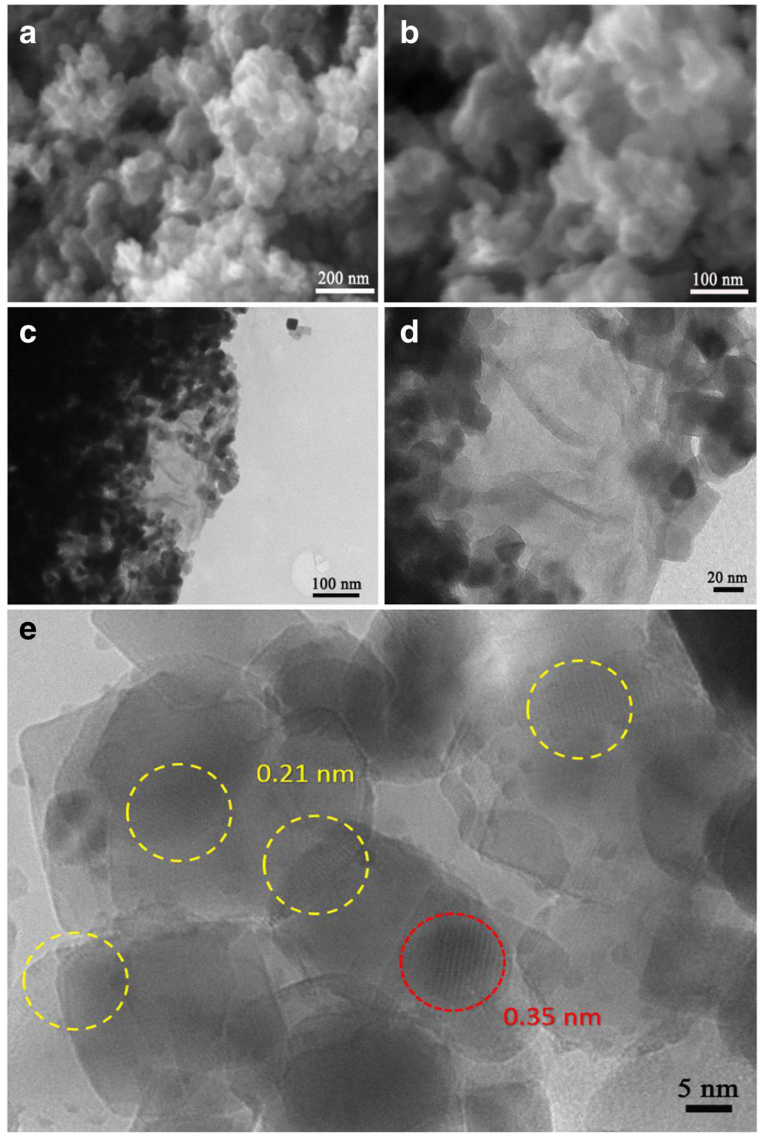

Fig. 1 **a** One hundred thousand times magnification and **b** 200,000 times magnification SEM pictures of RG–TiO_2 sample. **c** Thirty thousand times magnification and **d** 200,000 times magnification TEM pictures of RG–TiO_2 sample. **e** High-resolution TEM images of RG–TiO_2 sample

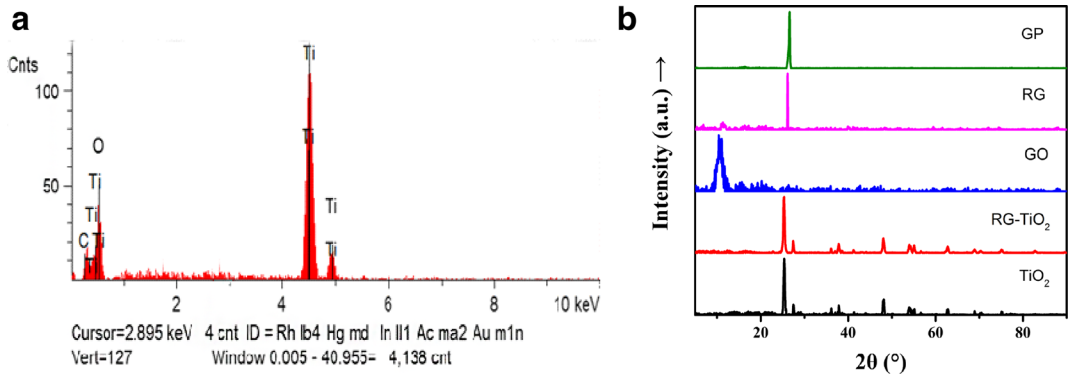

Fig. 2 **a** EDS analysis. **b** XRD patterns of samples

(101) plane of the TiO_2 anatase phase, while the areas circled using yellow long dash with a smaller lateral size of 0.21 nm were attributed to the graphene (100) planes.

The phase structures of GP, commercial TiO_2 P25, and self-prepared GO, RG, and RG–TiO_2 were characterized by powder XRD analysis (Fig. 2b). It can be found that both the GP and RG samples have a strong diffraction peak at $2\theta = 26.5°$, which was corresponding to graphene (002) facet. This result proved that the GO was successfully transferred into RG after the hydrothermal treatment. A (002) diffraction of GO was observed around $2\theta = 11.5°$ in the pattern of as-prepared GO. Facets (110, 101, 111) of the rutile TiO_2 and facets (101, 004, 200, 105, 211, 204, 116) of the anatase TiO_2 were found in both RG–TiO_2 and the TiO_2 P25, exactly confirming the content of TiO_2 P25. However, two facets of TiO_2 (101) and graphene (002) overlapped around 26.5 °C, making the recognition of them unsuccessful. Thus, there was no apparent difference between the patterns of RG–TiO_2 and TiO_2. Similar results were also confirmed by previous studies (Pan et al. 2015; Perera et al. 2012; Ramadoss and Kim 2013; Sher Shah et al. 2012; Zhang et al. 2011b). The tiny diffraction peaks of RG and RG–TiO_2, observed around 10° to 15°, may be ascribed to remaining unreduced GO in them.

The heterostructure was further evidenced by the Raman spectra of TiO_2, RG, and RG–TiO_2. In Fig. 3a, four Raman peaks of TiO_2 were found at around 144, 395, 512, and 639 cm^{-1}, matching four modes of TiO_2 as Eg(1), B1g(1), A1g + B1g(2), and Eg(2), respectively. For RG–TiO_2, the peak intensities of these four relevant modes were significantly decreased. Meanwhile, the Eg band of the RG–TiO_2 nanocomposite showed a blue shift, which was likely ascribed to the interfacial interaction between RG and TiO_2. The existence of the Ti–O–C bonds can make the TiO_2 lattice more compressed, and the more energy of phonons is gained by TiO_2's surface, the more blue shift there would be (Perera et al. 2012). Figure 3a also shows two typical peaks around 1345 and 1580 cm^{-1}, commonly corresponding to the D band of the sp3 defects and the G band of sp2 plane vibrations in RG and RG–TiO_2. Generally, the intensity ratio of D band and G band (ID/IG) generally represents the ratio of defects in graphene. More details of this interested spectrum range was magnified in the Fig. 3b. It was found that the ID/IG of RG was about 1.03, and increased to at about 1.12 in the RG–TiO_2. The increasing of ID/IG can be clearly attributed to the strong interfacial interaction between RG and TiO_2 in the RG–TiO_2, changing some of in plane sp2 C=C to the sp3 vibration. Moreover, a small bulge was observed in both the RG and the RG–TiO_2 around 2500–3000 cm^{-1}, which can be ascribed to the RG's 2D band. Since the RG was reduced from GO, some defects were expected to appear on the surface of RG as GO islands, leading these 2D bands as not very obvious.

In the FT-IR analysis (Fig. 3c), a broad low frequency absorption from 500 to 1000 cm^{-1} appears in both TiO_2 and RG–TiO_2 spectra, while not perfectly matched. This range could be attributed to Ti–O–Ti vibration, and a little fluctuation around 800 cm^{-1} of RG–TiO_2 sample was likely owing to the vibration of Ti–O–C bond

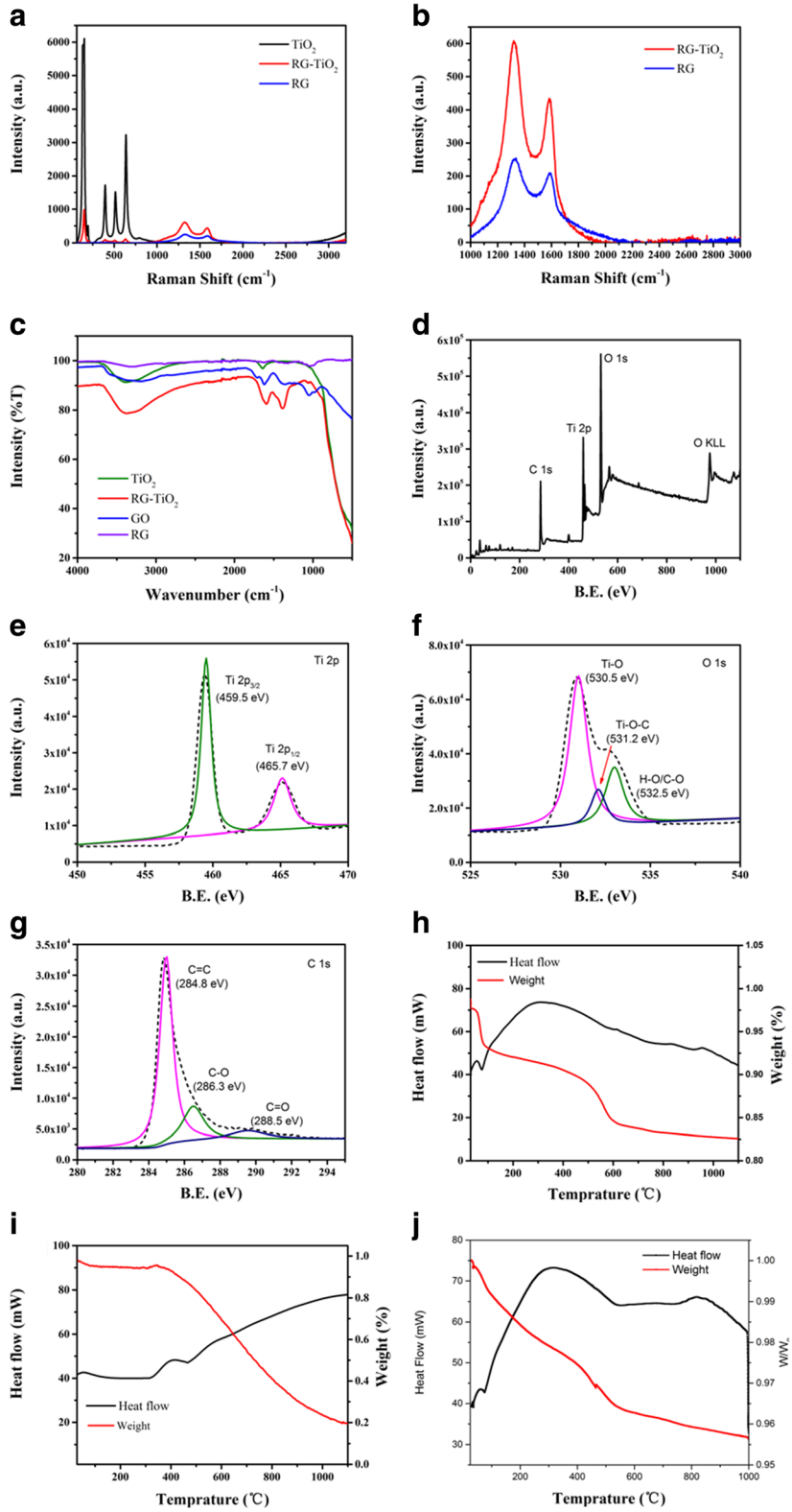

Fig. 3 **a** Overall and **b** detailed Raman spectra. **c** FT-IR spectra of TiO_2, RG–TiO_2, and RG. XPS survey spectrum of **d** RG–TiO_2, **e** Ti 2p, **f** O 1s, and **g** C 1s. Heat flow and weight loss curves of **h** RG–TiO_2, **i** RG, and **j** RG–TiO_2 physical mixtures in air atmosphere from room temperature to 1100 °C, with a heating rate of 10 °C min^{-1}

(usually at around 798 cm^{-1}). The absorption peaks around 1000 and 1480 cm^{-1} of RG and RG–TiO_2 could be attributed to the vibration of =C–H and conjugated C=C sp2, respectively, which illustrates that some GO has been successfully conversed into RG. Moreover, the vibration peaks of –OH (3371 cm^{-1}) in the spectra of the RG and RG–TiO_2 nanocomposite might be attributed to GO. However, since the same peak was also found in the spectrum of TiO_2, it may also possibly be attributed to the absorbed water molecules on materials surface. Actually, those functional groups on the surface of the original GO can not only offer spots for the TiO_2 nanoparticles to attach on, and then form Ti–O–C bonds, but these functional groups on the synthesized RG can also continuously help overcome strong interactions between individual RG sheets and then separating well in aqueous solution with GO islands on them.

To provide more detailed understanding towards the binding structures of the RG–TiO_2, a whole range XPS characterizations of RG–TiO_2 (Fig. 3d) were carried out, and the spectra of Ti 2p, O 1s and C 1s core levels are shown in the Fig. 3e–g. In the high-resolution Ti 2p spectrum, there were two peaks at bonding energies of 459.5 and 465.7 eV, which can be attributed to Ti 2p3/2 and Ti 2p1/3 of T4+ in TiO_2 respectively. In the core level analysis of O 1s, the peaks around 530.5, 531.2, and 532.5 eV can be assigned to bulk oxygen (O_2–) in TiO_2, O in Ti–O–C, and in H–O/C–O covalent bond, respectively. Similar results were evidenced in the previous work by Shuhua Yang et al. (Yang et al. 2015). In the core level analysis of C 1s, the C=C, C–O, and C=O evidenced in the aforementioned FT-IR and Raman spectra were also confirmed with corresponding banding energies at 284.8, 286.3, and 288.5 eV. (Yang et al. 2015) Among these three peaks, C=C was the strongest one as shown in Fig. 3g, which was certainly different from the high-resolution C 1s spectrum of GO, evidenced by an earlier study of Perera et al. (2012) Our XPS results matched the results of FT-IR and Raman relatively closely, and further proved that the hydrothermal treatment did convert some GOs into RG, and there were strong interfacial interactions Ti–O–C between TiO_2 and RG in the RG–TiO_2 nanocomposite. Moreover, no C–Ti bond at around 282 eV (C 1s) was observed, and it revealed that no carbon has doped into the lattice of TiO_2 (Huang et al. 2013) and the interfacial interaction between TiO_2 and RG can only be strengthened by the existence of Ti–O–C bond.

DSC and TGA results of RG and the RG–TiO_2 further support the existence of Ti–O–C bond (Fig. 3h, i). The experiments were carried out in air atmosphere from room temperature to 1100 °C, with a heating rate of 10 °C min^{-1}. As shown by the TGA of RG and RG–TiO_2, supported by the heat absorption peaks in their DSC curves, a great mass loss (~10%) appeared at around 100 °C corresponding to water evaporation. This was followed by a gradual mass loss in both RG and RG–TiO_2. After 550 °C, the mass of the RG–TiO_2 sharply dropped again, which was mostly likely attributed to RG's burning out, evidenced by the strong heat release valleys in its DSC curve. In comparison, the burning out temperature of RG by itself was around 400 °C. The thermal stability improvement of the RG in RG–TiO_2 nanocomposite was significant. As a contrast, we also made a RG–TiO_2 physical mixture sample. Not as the TGA result of RG–TiO_2 nanocomposite with Ti–O–C interfacial chemical bond, the one of RG–TiO_2 physical mixture sample showed that its burning out temperature was also around 400 °C, which proved that the significant thermal stability improvement of the RG in RG–TiO_2 nanocomposite was most likely due to the existence of strong Ti–O–C interfacial chemical bond.

Photocatalytic activity and mechanism

Improved charge carriers' migration

The charge carriers' migration behavior of the RG–TiO_2 nanocomposite was explored by measuring EIS, with TiO_2 P25 as the blank reference. As shown in the Nyquist plots of TiO_2 and RG–TiO_2 (Fig. 4a), at a high frequencies range which was closer to the origin, both TiO_2 and RG–TiO_2 gave out a shape of quadrant, and the radius of TiO_2's quadrant was clearly larger than the one of the RG–TiO_2s. The radii of the quadrants can reflect charge transfer resistance, and the material with larger radius is supposed to have relatively larger resistance. It can be expected that the existence of RG on the surface of RG–TiO_2 nanocomposite helped TiO_2 reduce the charge transfer resistance across the solid–liquid junction. This result can be assigned to the fact that RG is more conductive than TiO_2. Since the concentration of charge carriers in semiconductors is always far lower than metals and even lower than electrolyte solution, most of the voltage applies to the semiconductors themselves rather than to the solid–liquid surface, and, consequently, some of the charges in electrolyte solution

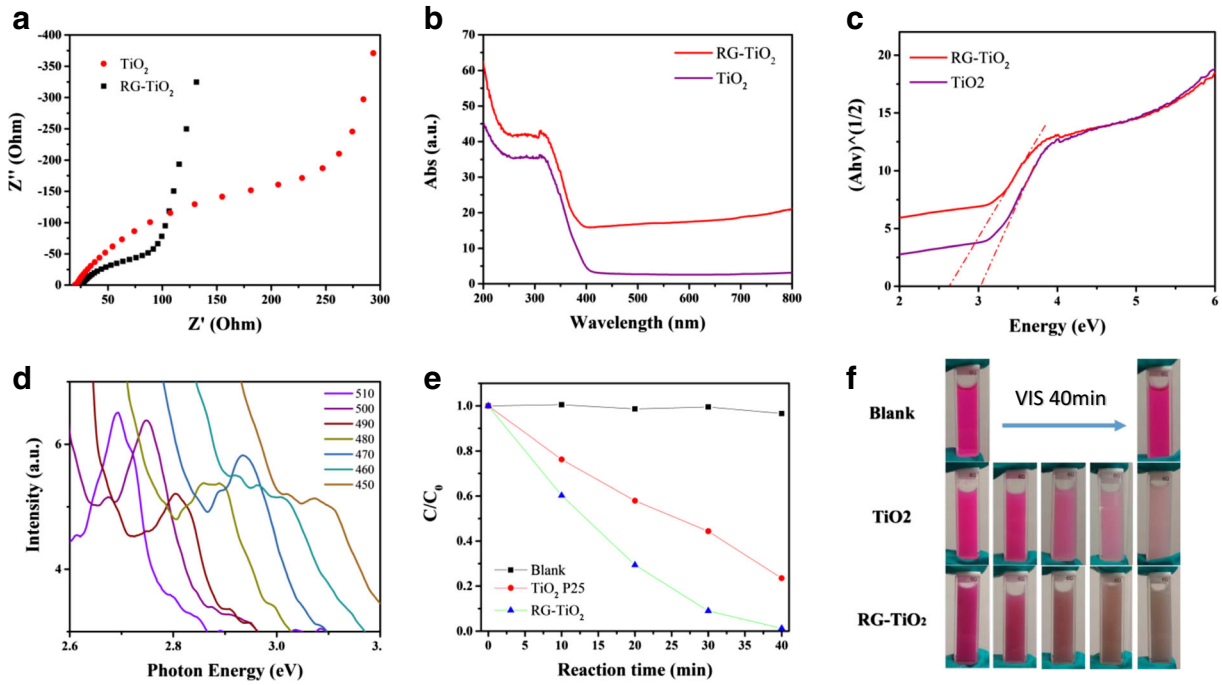

Fig. 4 **a** Nyquist plots of the TiO_2 and RG–TiO_2 samples. **b** UV–Vis DRS and **c** relationship between $(Ah\nu)^{0.5}$ and hν. **d** PL spectra of RG–TiO_2 nanocomposite at different excitation wavelengths. **e** Photodegradation of Rh. B, where C_0 is the initial concentration of Rh. B and *C* is the concentration of Rh. B after irradiation of the sample in the corresponding time interval. **f** Images of Rh. B degradation states: from initial solutions to the solutions after 40 min. The photos were taken without centrifugation

cannot be balanced. This means the charge carriers' migration in the semiconductors can finally determine the charge transfer kinetics and rate. The reduced charge transfer resistance of the RG–TiO_2 over TiO_2 is expected to help transferring electrons and holes between nanocomposite and electrolyte solution, enhancing the separation of photogenerated electrons and holes, and subsequently prolonging the lifetime of photogenerated electrons and holes.

Visible light absorption

The UV–Vis DRS and the corresponding relationship between $(Ah\nu)^{1/2}$ and hν were performed to examine the photocatalytic activities of TiO_2 and the RG–TiO_2. As shown in the Fig. 4b, both TiO_2 and RG–TiO_2 had photoresponses to UV and visible light. However, in the whole range of visible light, the light absorption of RG–TiO_2 was always better than TiO_2 P25 alone. Since only about 3–5% of sunlight is in UV range, the enhanced visible light absorption was supposed to use sunlight more effectively and then improve the photocatalytic properties of TiO_2.

Moreover, since TiO_2 has an indirect bandgap, the optical absorption near the band edge follows the Kubelka–Munk function (Anderson and Bard 1997):

$$h\nu = A\,(h\nu - Eg)^{1/2}$$

wher h represents Planck constant, ν represents the light frequency, Eg represents the bandgap and *A* is a constant. Hence, after a series of formula transformations, the bandgap of TiO_2 and RG–TiO_2 determined by the Kubelka–Munk equation (Fig. 4c) was about 3.1 and 2.6 eV, respectively. Obviously, the bandgap of RG–TiO_2 was significantly narrowed down compared to TiO_2 P25 itself. Similar results were also found by other groups (Fan et al. 2011; Long et al. 2013; Ong et al. 2014; Zhang et al. 2010). By having narrower bandgap, compared to TiO_2, the photoresponse range of RG–TiO_2 nanocomposites clearly changed from UV (~390 nm) to visible light (~480 nm), which also offers a potential utilization of visible light.

The narrowed down bandgap of RG–TiO_2 nanocomposite was most likely attributed to the Ti–O–C bond between TiO_2 nanoparticles and RG sheets, which

causes an intimate interaction, similar to the carbon-doped TiO_2 composites (Fan et al. 2011; Huang et al. 2013; Pan et al. 2012; Yang et al. 2015; Zhang et al. 2009). RG can act as sensitizers to enable large bandgap semiconductors utilizing visible light (Chen and Wang 2014). If TiO_2 nanoparticles and RG sheets were chemically coupled, the available graphene functions as lowering the bottom of conduction band (CB) of TiO_2. The interfacial electron transferring and electron–holes' separation can be then efficiently facilitated.

In addition, an up-conversion photoluminescence (UCPL) effect of RG should also provide a synergic explanation to this improvement of light absorption. According to published studies, UCPL is a phenomenon that the photon energy of emission is higher than that of excitation, which has been widely reported with solid-state materials doped with rare earth elements, semiconductors with heterostructures, quantum dots, etc. (Ha et al. 2015) Recently, normal PL as well as UCPL features of carbon quantum dots, graphene quantum dots, and graphene oxide quantum dots have been well characterized (Gan et al. 2013; Hu et al. 2015; Liu et al. 2013; Zhu et al. 2015; Zhuo et al. 2012). By mentioning RG quantum dots, it refers to not only the actual dots with size smaller than 10 nm but also the graphene sheets with graphene oxide quantum islands on it (Gómez-Navarro et al. 2007; Kaiser et al. 2009; Loh et al. 2010). From the results of this study, FT-IR, Raman, and XPS, it can be found that a small amount of oxygen groups does exist on the surface of RG–TiO_2 nanocomposite. Therefore, this nanocomposite can be seen as a RG quantum structure material. In the PL spectra of RG–TiO_2 (Fig. 4d), though the intensity of those emission peaks were not extremely high, it can be found that when the nanocomposite was excited using a 450-nm light (~2.6 eV), the emission peak appeared at around 3.1 eV (390 nm), which corresponded exactly to the DRS result. The reason why the intensity of 3.1 eV peak was so weak may be due to its being absorbed and utilized by TiO_2 nanoparticles. The mechanism of RG–TiO_2 nanocomposite's UCPL was schemed in the Fig. 5a. Normally, the visible light with wavelength larger than 420 nm is not able to be used by TiO_2 materials alone (the absorbable light wavelength limitation of the rutile TiO_2 is 414 nm, while the one of the anatase TiO_2 is 388 nm) (Zhuo et al. 2012). However, the visible light within this range can excite RG quantum material and transfer a light with wavelength of 450 to 390 nm by an UCPL effect, which is then able to be utilized by TiO_2. Thus, the wavelength limitation of

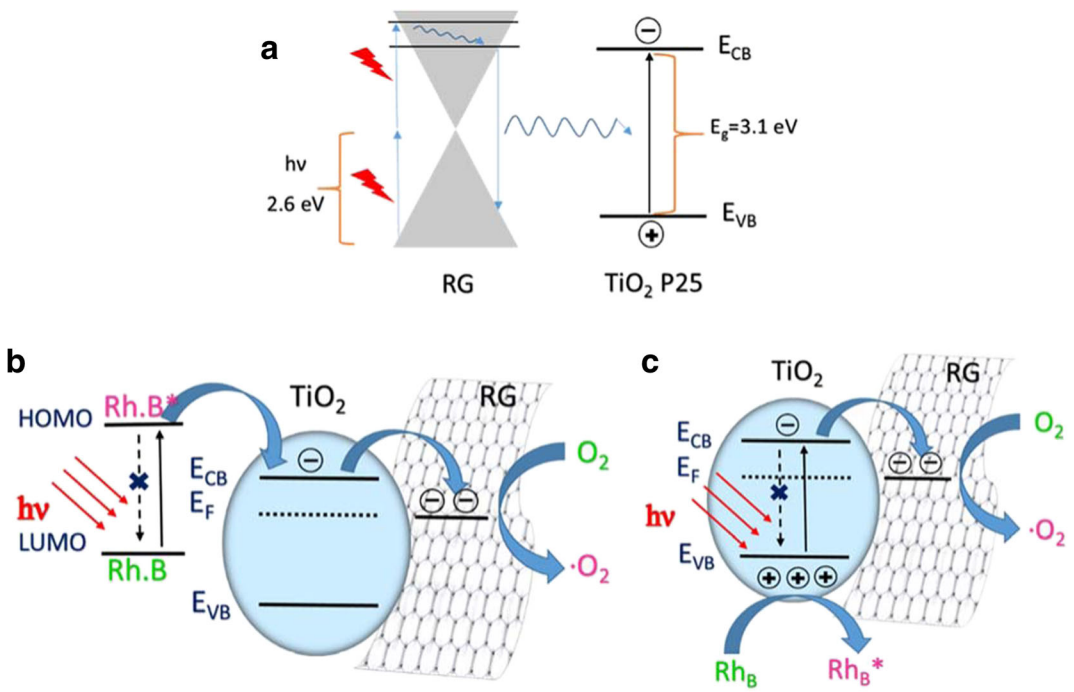

Fig. 5 Schematic of **a** UCPL mechanism for RG–TiO_2 nanocomposite under visible light (hν ~2.6 eV) irradiation, and **b**, **c** schematics of proposed mechanism of Rh. B photodegradation

absorbable light is accordingly changed. A recent new literature even illustrated the possibility of the improvement of the charge separation by the hydrothermal treated P25 (Ide et al. 2016). As mentioned in this reference, such as "the hydrothermal treatment of P25 TiO_2 selectively converts the amorphous component into crystalline TiO_2 on the interfaces of the original anatase and rutile components." This was partially coincided with our current results. Actually, we found not only the improvement of the charge separation but also the change of the bandgap.

Enhanced degradation of Rh. B

The photocatalytic performance of as-prepared RG–TiO_2 nanocomposite was then investigated by evaluating the photodegradation of Rh. B (Xe light source, room temperature, ambient pressure). From the images of the Rh. B degradation results (Fig. 4f) in three different situations—Rh. B solution without any photocatalyst, Rh. B solution with TiO_2 P25, and Rh. B solution with RG–TiO_2 nanocomposite—it was revealed that Rh. B itself did not photodegrade at all, and the photodegradation result of Rh. B with TiO_2 P25 was not as good as it was with RG–TiO_2. These initial results were proved further by the UV–Vis absorption measurements (Fig. 4e). In the RG–TiO_2 aided case, the characteristic peak of Rh. B at 554 nm decayed rapidly and nearly disappeared completely after 40 min. In comparison, after 40 min of light exposure with TiO_2 P25 nanoparticles as the photocatalyst, there was still 20% of the Rh. B in the solution. Since the rate of Rh. B photodegradation with catalysts agrees well with the pseudo-first-order kinetics, an integrated rate equation is suggested as follows: $\ln (C_0/C_t) = kt$, where C_0 and C_t are initial concentration and the concentration of Rh. B at time t, and k is the apparent degradation rate constant (Sher Shah et al. 2012). Thus, based on the data in Fig. 4e, the calculated rate constants of the TiO_2 P25 and RG–TiO_2 were 0.0255 and 0.0602 min^{-1} respectively. That is to say, the RG junction on TiO_2 promoted the reaction rate by about three times.

Considering that Rh. B can be stimulated by visible light towards its excited state (Rh. B^*) and give out electrons, why did the blank sample not degrade at all after 40 min visible light exposure? There were likely two clues underlying this phenomenon. Firstly, the absorbed oxidizing agents on Rh. B (such as dissolved oxygen) was very limited, resulting in inefficient giving out of the photogenerated electrons from Rh. B. Secondly, the lifetime of the Rh. B^* can be very short (Strickler and Berg 1962), and it can recombine with photogenerated electrons very quickly and form the Rh. B molecules again. Thus, though some Rh. B molecules can surely be excited by visible light, not very much difference can finally happen.

Another interesting thing needs to be pointed out is that the BET surface area of TiO_2 P25 was measured as 49.1856 $m^2\ g^{-1}$ while the one of RG–TiO_2 was 31.5453 $m^2\ g^{-1}$. The decreased BET surface area of the RG–TiO_2 nanocomposite may be according to the clustering of TiO_2 nanoparticles in the RG–TiO_2 nanocomposite covered by RG sheets. Thus, according to these results, the improved photocatalytic activity of RG–TiO_2 nanocomposite over TiO_2 nanoparticles cannot be straightforwardly relevant to their surface area, but should be relevant to the improved conductivity and bandgap structure.

Overall, the mechanism of the enhanced photodegradation of Rh. B with RG–TiO_2 as the photocatalyst can be schemed in two aspects: (1) dye molecules were attached to TiO_2 nanoparticles and excited (Fig. 5b), and (2) dye molecules were attached to TiO_2 nanoparticles, and TiO_2 nanoparticles were excited (Fig. 5c). The possible degradation intermediates of Rh. B during the photocatalytic process are shown in Fig. 6.

When the attached Rh. B molecules on TiO_2 nanoparticles are excited by visible light, the mechanism is similar to the anodic reaction of the DSSC (Wang et al. 2013). To be specific, the photosensitized dye molecules absorb sunlight and create a high-energy state, from which a photoexcited electron is injected into the CB of TiO_2 (Wu and Zhu 2013). Because of the two-dimensional π-conjugation structure on RG sheets which is working as an electron acceptor, and an interfacial Ti–O–C chemical bond which connects TiO_2 with RG relatively well, the photoexcited electrons can be quickly transferred from the CB of TiO_2 to RG (Sher Shah et al. 2012). The electrons stored by RG will then be used by O_2 dissolved in solution. The main reactions are shown as follows.

$$\mathrm{Rh.B} + h\nu \rightarrow \mathrm{Rh.B}^* + e^-$$

$$\mathrm{TiO_2} + e^- \rightarrow \mathrm{TiO_2}(e^-)$$

$$\mathrm{TiO_2}(e^-) + \mathrm{RG} \rightarrow \mathrm{TiO_2} + \mathrm{RG}\,(e^-)$$

$$\mathrm{RG}\,(e^-) + \mathrm{O_2} \rightarrow \mathrm{RG} + \mathrm{O_2}^-$$

On the other hand, thanks to a lower bandgap and the UCPL effect of RG, RG–TiO_2 nanocomposite has an

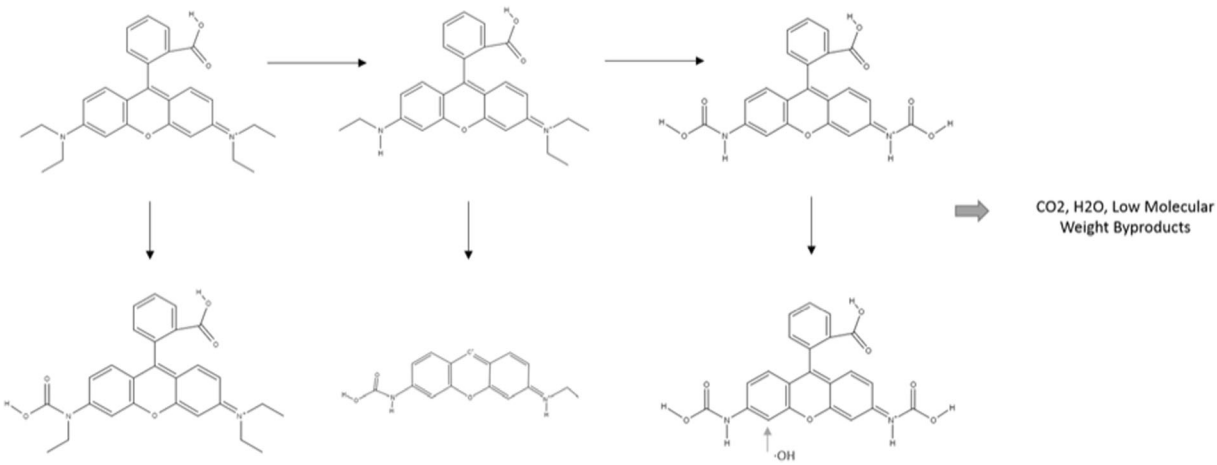

Fig. 6 Schematic of the possible degradation intermediates of Rh. B during the photocatalytic process (Cotto-Maldonado et al. 2013)

obvious red shift in light absorption compared to TiO_2 nanoparticles. Therefore, when TiO_2 nanoparticles are stimulated, the electrons in the valence band (VB) of TiO_2 can jump into its CB and the photogenerated electron–hole pairs are then formed. From previous study, RG has a near-zero bandgap (Freitag 2008) and a large work function (~4.5 eV) (Ma et al. 2014; Yu et al. 2009), while the CB of TiO_2 is about ca. −4.21 eV (Kapilashrami et al. 2014; Ma et al. 2014). Thus, Schottky junctions are formed between TiO_2 nanoparticles and RG sheets, which may lead to efficient charges' separation by transferring photogenerated electrons from TiO_2 to RG sheets (Ma et al. 2014). By having this Schottky junction, the rate of recombination of the photogenerated electron–hole pairs decreases significantly, which consequently enhances the photocatalytic activity. Then, the electrons on the surface of RG are trapped by the adsorbed molecular oxygen to produce superoxide anion ($\cdot O_2^-$) radicals (Pan et al. 2015). The mechanism of dye degradation then mainly follows two routes (Sher Shah et al. 2012): the holes on the VB of TiO_2 can directly oxidize Rh. B molecules to their excited states, and the photogenerated holes on the VB of TiO_2 can also transfer hydroxyl radicals into hydroxyl groups, which then degrade dye molecules which then become hydroxyl radicals again. The main reactions are shown as follows.

$$TiO_2 + h\nu \rightarrow TiO_2(h^+) + e^-$$

$$e^- + RG \rightarrow RG\,(e^-)$$

$$RG\,(e^-) + O_2 \rightarrow RG + O_2^-$$

$$TiO_2(h^+) + H_2O/OH^- \rightarrow TiO_2 + \cdot OH$$

$$OH + Rh.B \rightarrow Rh.B^* + H_2O/OH^-$$

or

$$TiO_2(h^+) + Rh.B \rightarrow Rh.B^* + TiO_2$$

Conclusion

In this study, we prepared a RG–TiO_2 nanocomposite using a simple hydrothermal method starting from the commercial TiO_2 P25 and the liquid exfoliated GO. The multiple characterizations of this nanocomposite confirmed that GO was successfully transferred into RG, and a Ti–O–C band was formed in the interface between TiO_2 nanoparticle and RG sheets. With these benefits, as-prepared RG–TiO_2 nanocomposite exhibits a narrower bandgap (2.6 eV) contrasting to TiO_2 P25 (3.1 eV), leading a greatly improved photocatalytic efficiency in the photodegradation of Rh. B compared to TiO_2 P25. The excellent effects which RG sheet played on TiO_2 nanoparticle, which led to enhanced photocatalytic properties, were identified as prompt injection of photogenerated electrons from the CB of TiO_2 into RG, improved separation of photogenerated electron–hole pairs, and the likelihood of the UCPL effect provided by RG quantum structure. This study also suggested the possibility of visible light photodegradation applications by forming the heterojunction structure of metal oxide with RG.

Acknowledgment This study was supported by the 2014–2015 NSF RSP EPSCoR program, 2015–2017 NSF REG, and RSP EPSCoR program (the National Science Foundation under Cooperative Agreement No. 1355438), as well as the support from the

NSF–CHE–MRI under the Award ID of 1338072. Authors also extend our acknowledgement to partial support by the US Department of Agriculture (5040-12630-004-00D). Additionally, the authors also very much appreciate the help from Dr. Sanju Gupta (sanju.gupta@wku.edu)—Raman tests, Dr. John Andersland (john.andersland@wku.edu)—electron microscope training, Dr. Hanjing Tian (htian@mail.wvu.edu)—XPS tests, and Mr. Craig Clark (william.clark927@topper.wku.edu)—proofreading.

Compliance with ethical standards

Conflict of interest The authors declare that they have no conflict of interest.

References

Anandan S, Narasinga Rao T, Sathish M, Rangappa D, Honma I, Miyauchi M (2012) Superhydrophilic graphene-loaded TiO2 thin film for self-cleaning applications. ACS Appl Mater Interfaces 5:207–212

Anderson C, Bard AJ (1997) Improved photocatalytic activity and characterization of mixed TiO2/SiO2 and TiO2/Al2O3 materials. J Phys Chem B 101:2611–2616

Chen H, Wang L (2014) Nanostructure sensitization of transition metal oxides for visible-light photocatalysis. Beilstein J Nanotechnol 5:696–710

Chien SC, Chang C, Chen S, Wang M, Rao MM, Veni SS (2011) Effect of sunlight irradiation on photocatalytic pyrene degradation in contaminated soils by micro-nano size TiO 2. Sci Total Environ 409:4101–4108

Cotto-Maldonado MDC, Campo T, Elizalde E, Gómez-Martínez A, Morant C, Márquez F (2013) Photocatalytic degradation of Rhodamine-B under UV-visible light irradiation using different nanostructured catalysts. Am Chem Sci J 3:178–202

Cozzoli PD, Fanizza E, Comparelli R, Curri ML, Agostiano A, Laub D (2004) Role of metal nanoparticles in TiO2/Ag nanocomposite-based microheterogeneous photocatalysis. J Phys Chem B 108:9623–9630

Fan W, Lai Q, Zhang Q, Wang Y (2011) Nanocomposites of TiO2 and reduced graphene oxide as efficient photocatalysts for hydrogen evolution. J Phys Chem C 115:10694–10701

Freitag M (2008) Graphene: nanoelectronics goes flat out. Nat Nanotechnol 3:455–457

Fujishima A, Honda K (1972) TiO2 photoelectrochemistry and photocatalysis. Nature 238:37–38

Gan Z, Wu X, Zhou G, Shen J, Chu PK (2013) Is there real upconversion photoluminescence from graphene quantum dots? Advanced Opt Mater 1:554–558

Gómez-Navarro C, Weitz RT, Bittner AM, Scolari M, Mews A, Burghard M, Kern K (2007) Electronic transport properties of individual chemically reduced graphene oxide sheets. Nano Lett 7:3499–3503

Zhu HY, Lan Y, Gao XP, Ringer SP, Zheng ZF, Song a DY, Zhao JC (2005) Phase transition between nanostructures of titanate and titanium dioxides via simple wet-chemical reactions. J Am Chem Soc 127:6730–6736

Ha HD, Jang M-H, Liu F, Cho Y-H, Seo TS (2015) Upconversion photoluminescent metal ion sensors via two photon absorption in graphene oxide quantum dots. Carbon 81:367–375

Hu Y, Yang J, Tian J, Jia L, Yu J-S (2015) Oxygen-driven, high-efficiency production of nitrogen-doped carbon dots from alkanolamines and their application for two-photon cellular imaging. RSC Adv 5:15366–15373

Huang Q et al (2013) Enhanced photocatalytic activity of chemically bonded TiO2/graphene composites based on the effective interfacial charge transfer through the C–Ti bond. ACS Catal 3:1477–1485

Ide Y, Inami N, Hattori H, Saito K, Sohmiya M, Tsunoji N, Komaguchi K, Sano T, Bando Y, Golberg D, Sugahara Y (2016) Remarkable charge separation and photocatalytic efficiency enhancement through interconnection of TiO_2 nanoparticles by hydrothermal treatment. Angew Chem Int Ed 55(11):3600–3605

Jiang G et al (2011) TiO 2 nanoparticles assembled on graphene oxide nanosheets with high photocatalytic activity for removal of pollutants. Carbon 49:2693–2701

Jiang Y, Wang W-N, Biswas P, Fortner JD (2014) Facile aerosol synthesis and characterization of ternary crumpled graphene–TiO2–magnetite nanocomposites for advanced water treatment. ACS Appl Mater Interfaces 6:11766–11774

Kaiser AB, Gómez-Navarro C, Sundaram RS, Burghard M, Kern K (2009) Electrical conduction mechanism in chemically derived graphene monolayers. Nano Lett 9:1787–1792

Kapilashrami M, Zhang Y, Liu Y-S, Hagfeldt A, Guo J (2014) Probing the optical property and electronic structure of TiO2 nanomaterials for renewable energy applications. Chem Rev 114:9662–9707

Kim Y-G, Walker J, Samuelson LA, Kumar J (2003) Efficient light harvesting polymers for nanocrystalline TiO2 photovoltaic cells. Nano Lett 3:523–525

Liao D, Badour C, Liao B (2008) Preparation of nanosized TiO2/ZnO composite catalyst and its photocatalytic activity for degradation of methyl orange. J Photochem Photobiol A Chem 194:11–19

Liu F, Jang MH, Ha HD, Kim JH, Cho YH, Seo TS (2013) Facile synthetic method for pristine graphene quantum dots and graphene oxide quantum dots: origin of blue and green luminescence. Adv Mater 25:3657–3662

Loh KP, Bao Q, Eda G, Chhowalla M (2010) Graphene oxide as a chemically tunable platform for optical applications. Nat Chem 2:1015–1024

Long M, Qin Y, Chen C, Guo X, Tan B, Cai W (2013) Origin of visible light photoactivity of reduced graphene oxide/TiO2 by in situ hydrothermal growth of undergrown TiO2 with graphene oxide. J Phys Chem C 117:16734–16741

Ma Y, Wang X, Jia Y, Chen X, Han H, Li C (2014) Titanium dioxide-based nanomaterials for photocatalytic fuel generations. Chem Rev 114:9987–10043

Marcano DC et al (2010) Improved synthesis of graphene oxide. ACS Nano 4:4806–4814

Mir NA, Khan A, Muneer M, Vijayalakhsmi S (2013) Photocatalytic degradation of a widely used insecticide Thiamethoxam in aqueous suspension of TiO2: adsorption, kinetics, product analysis and toxicity assessment. Sci Total Environ 458:388–398

Ong W-J, Tan L-L, Chai S-P, Yong S-T, Mohamed AR (2014) Self-assembly of nitrogen-doped TiO2 with exposed {001}

facets on a graphene scaffold as photo-active hybrid nanostructures for reduction of carbon dioxide to methane. Nano Res 7:1528–1547

Pan D et al (2015) Efficient separation of electron-hole pairs in graphene quantum dots by TiO2 heterojunctions for dye degradation. ACS Sustainable Chemistry & Engineering

Pan X, Zhao Y, Liu S, Korzeniewski CL, Wang S, Fan Z (2012) Comparing graphene-TiO2 nanowire and graphene-TiO2 nanoparticle composite photocatalysts. ACS Appl Mater Interfaces 4:3944–3950

Pelizzetti E, Carlin V, Minero C, Pramauro E, Vincenti M (1992) Degradation pathways of atrazine under solar light and in the presence of TiO2 colloidal particles. Sci Total Environ 123: 161–169

Perera SD, Mariano RG, Vu K, Nour N, Seitz O, Chabal Y, Balkus KJ Jr (2012) Hydrothermal synthesis of graphene-TiO2 nanotube composites with enhanced photocatalytic activity. ACS Catal 2:949–956

Qian W, Greaney PA, Fowler S, Chiu S-K, Goforth AM, Jiao J (2014) Low-temperature nitrogen doping in ammonia solution for production of N-doped TiO2-hybridized graphene as a highly efficient photocatalyst for water treatment. ACS Sustain Chem Eng 2:1802–1810

Ramadoss A, Kim SJ (2013) Improved activity of a graphene–TiO 2 hybrid electrode in an electrochemical supercapacitor. Carbon 63:434–445

Sher Shah MSA, Park AR, Zhang K, Park JH, Yoo PJ (2012) Green synthesis of biphasic TiO2–reduced graphene oxide nanocomposites with highly enhanced photocatalytic activity. ACS Appl Mater Interfaces 4:3893–3901

Strickler S, Berg RA (1962) Relationship between absorption intensity and fluorescence lifetime of molecules. J Chem Phys 37:814–822

Subramanian V, Wolf EE, Kamat PV (2003) Influence of metal/metal ion concentration on the photocatalytic activity of TiO2-Au composite nanoparticles. Langmuir 19:469–474

Sun Z, Chang H (2014) Graphene and graphene-like two-dimensional materials in photodetection: mechanisms and methodology. ACS Nano 8:4133–4156

Tributsch H (1972) Reaction of excited chlorophyll molecules at electrodes and in photosynthesis. Photochem Photobiol 16: 261–269

Wang P et al (2013) Dye-sensitization-induced visible-light reduction of graphene oxide for the enhanced TiO2 photocatalytic performance. ACS Appl Mater Interfaces 5:2924–2929

Wang SC, Yun JH, Luo B, Butburee T, Peerakiatkhajohn P, Thaweesak S, Xiao M, Wang LZ (2017) Recent progress on visible light responsive heterojunctions for photocatalytic applications. J Mater Sci Technol 33(1):1–22

Wu T, Liu G, Zhao J, Hidaka H, Serpone N (1998) Photoassisted degradation of dye pollutants. V. Self-photosensitized oxidative transformation of rhodamine B under visible light irradiation in aqueous TiO2 dispersions. J Phys Chem B 102: 5845–5851

Wu Y, Zhu W (2013) Organic sensitizers from D–π–A to D–A–π–A: effect of the internal electron-withdrawing units on molecular absorption, energy levels and photovoltaic performances. Chem Soc Rev 42:2039–2058

Xiang Q, Yu J, Jaroniec M (2012) Graphene-based semiconductor photocatalysts. Chem Soc Rev 41:782–796

Yamashita H et al (1994) Photocatalytic reduction of CO2 with H2O on TiO2 and Cu/TiO2 catalysts. Res Chem Intermed 20:815–823

Yang S, Lin Y, Song X, Zhang P, Gao L (2015) Covalently coupled ultrafine H-TiO2 nanocrystals/nitrogen-doped graphene hybrid materials for high-performance supercapacitor. ACS Appl Mater Interfaces 7:17884–17892

Yu Y-J, Zhao Y, Ryu S, Brus LE, Kim KS, Kim P (2009) Tuning the graphene work function by electric field effect. Nano Lett 9:3430–3434

Zhang H, Lv X, Li Y, Wang Y, Li J (2009) P 25-graphene composite as a high performance photocatalyst. ACS Nano 4:380–386

Zhang H, Xu P, Du G, Chen Z, Oh K, Pan D, Jiao Z (2011a) A facile one-step synthesis of TiO2/graphene composites for photodegradation of methyl orange. Nano Res 4:274–283

Zhang Y, Tang Z-R, Fu X, Xu Y-J (2010) TiO2–graphene nanocomposites for gas-phase photocatalytic degradation of volatile aromatic pollutant: is TiO2–graphene truly different from other TiO2–carbon composite materials? ACS Nano 4:7303–7314

Zhang Y, Tang Z-R, Fu X, Xu Y-J (2011b) Engineering the unique 2D mat of graphene to achieve graphene-TiO2 nanocomposite for photocatalytic selective transformation: what advantage does graphene have over its forebear carbon nanotube? ACS Nano 5:7426–7435

Zheng XT, Ananthanarayanan A, Luo KQ, Chen P (2015) Glowing graphene quantum dots and carbon dots: properties, syntheses, and biological applications. Small 11:1620–1636

Zhu S, Song Y, Zhao X, Shao J, Zhang J, Yang B (2015) The photoluminescence mechanism in carbon dots (graphene quantum dots, carbon nanodots, and polymer dots): current state and future perspective. Nano Res 8:355–381

Zhu S et al (2012) Graphene quantum dots with controllable surface oxidation, tunable fluorescence and up-conversion emission. RSC Adv 2:2717–2720

Zhuo S, Shao M, Lee S-T (2012) Upconversion and downconversion fluorescent graphene quantum dots: ultrasonic preparation and photocatalysis. ACS Nano 6:1059–1064